

paMELA - Photoacoustic Melanoma Detector Design for Real-Time Imaging of Melanin with 18 db SNR and 10 μm Precision

Elia Arturo Vallicelli¹^a, Giberto Chirico¹^b, Oliver Cosmi¹, Lorenzo Stevenazzi¹
and Mattia Tambaro²^c

¹University of Milano, Bicocca, Milano, Italy

²University of Padova, Padova, Italy

Keywords: Photoacoustics, Analog Front-end, Digital Signal Processing.

Abstract: This article presents the complete photon-to-bit cross-domain model of a photoacoustic melanoma detector (paMELA), consisting of a pulsed laser, a multichannel acoustic sensor, an analog front-end and a DSP stage for the implementation of an acoustic imaging algorithm. The photoacoustic effect can be exploited to obtain complementary information on a suspected melanoma with respect to classical dermatoscopic techniques. By modelling the physical phenomena (generation and propagation of the acoustic signal), electromechanical process (pressure-voltage transduction by the acoustic sensor), the analog and digital signal processing, it is possible to evaluate the impact of each stage on the quality of the final image. Finally, the simulation results of paMELA allow to evaluate the performance of the detector in terms of localization precision and signal-to-noise ratio, using both a single point-like source and a complete biological tissue phantom with different sources sizes and features, obtaining 18 dB of SNR and 10 μm of precision in 1s acquisition.

1 INTRODUCTION

Melanoma is an aggressive malignant tumor that initially develops on the epidermis and subsequently expands deep into the tissues until it generates metastases. Although it represents a small percentage of skin cancers (<10%), it is responsible for 75% of deaths in the entire category (Stewart, 2003). The average onset is also young: it is the third most frequent cancer under the age of 50 and the highest cost in terms of years not lived. Between 2008 and 2016, melanoma represented the cancer with the greatest annual average increase in Italy, with + 8.8% in total in men and + 7.1% in women. If diagnosed in the early stages, treatment involves simple surgical excision with a 5-year survival rate of 98.4%. In the more advanced stages, however, when the melanoma has grown in depth to reach the dermis and lymphatic vessels, the risk of metastasis is very high. The 5-year survival rate drops drastically, reaching 63% if metastases are present in the regional lymph nodes and 22% if distant metastases are present making

necessary treatments that are invasive for the patient (chemotherapy, radiotherapy) and with high costs for health systems. An early diagnosis of melanoma is therefore of fundamental importance in order to be able to recognize it, have a favorable prognosis, minimally invasive treatment and a reduction in the associated socio-economic impact. Currently, the screening of melanomas is carried out by a specialized dermatologist who performs a visual inspection of the skin nevi using the dermatoscope (magnifying glass with polarized light, Figure (1), evaluating their morphological aspects, that is, shape, size and color.

In the event of a suspicious situation, surgical removal and histological examination of the tissue sample is carried out to assess the possible presence of melanoma and its thickness (Figure 1). Staging is in fact defined according to thickness since melanomas in the initial stages are found only in the epidermis (superficial layer), while in the more advanced stages they begin to penetrate the dermis (vascularized underlying layer), with the possibility

^a <https://orcid.org/0000-0003-0905-151X>

^b <https://orcid.org/0000-0001-6578-6460>

^c <https://orcid.org/0000-0002-7593-5084>

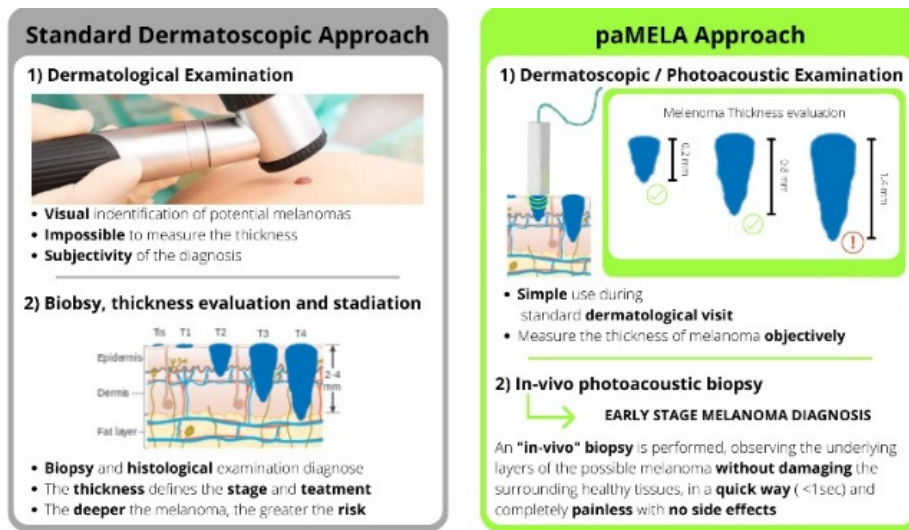


Figure 1: Comparison between standard dermatoscopic technique and photoacoustic technique.

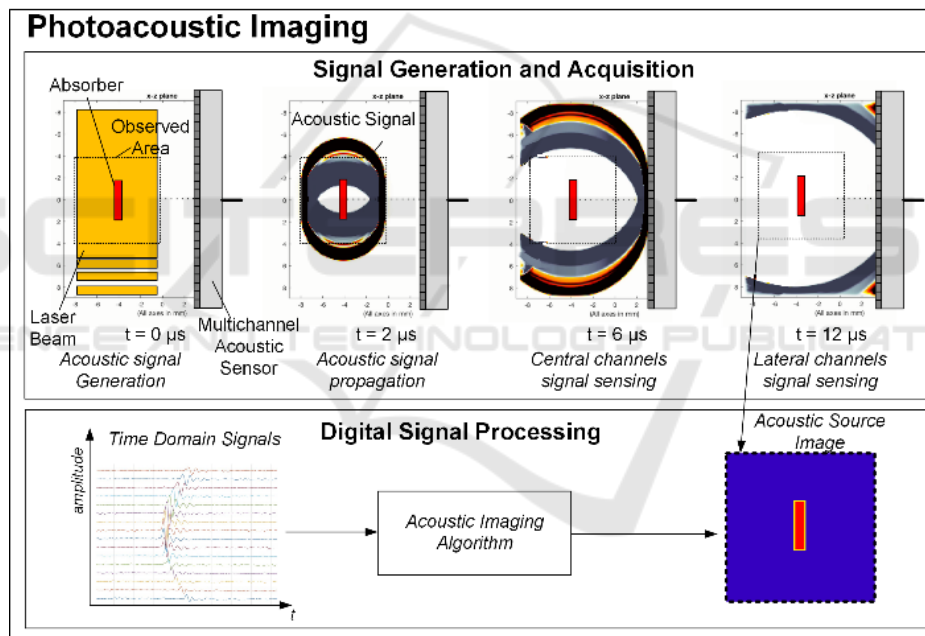


Figure 2: Photoacoustic imaging process.

of generating metastases. It is therefore known that measuring the thickness of melanoma is of fundamental importance for an early diagnosis and an effective clinical approach. However, this is not possible with standard dermatoscopy which is limited to observing the surface morphological characteristics to identify suspected cases to be surgically removed, postponing the staging to the next histological examination and strongly depending on the experience of the dermatologist.

An emerging alternative technique for the study of melanomas is based on photoacoustics. When a

light pulse radiates an optical absorber, the rapid deposition of energy generates an increase in temperature and pressure that propagates in the medium like an acoustic wave (Figure 2).

This acoustic wave can be acquired by a dedicated acoustic detector to obtain information on the absorber that generated it. By exploiting the sound generated by a suspect melanoma it is possible to obtain information on its morphology and in particular on its thickness (Zhou 2014, Sinnamon 2019). With this technique, during a simple

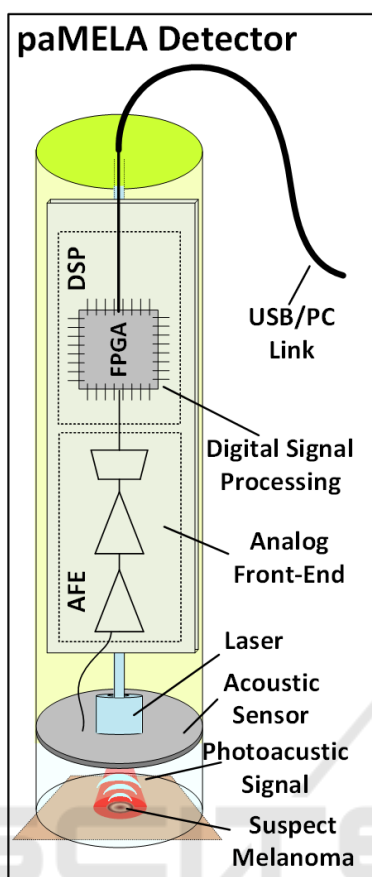


Figure 3: Block scheme of paMELA.

dermatological examination, it is possible to perform a quick and painless in-vivo biopsy, which allows to evaluate the actual presence and stage of melanoma (Wang 2016, Park 2021). The photoacoustic effect can be used to observe a wide range of biological systems and the photoacoustic instruments currently on the market are general-purpose to adapt to different research needs, therefore not being optimized for melanomas.

For these reasons, this work presents the design and simulation characterization of paMELA (photoacoustic melanoma detector), a compact real-time photoacoustic detector optimized for characterizing melanoma. This work is organized as follows. Section II describes the design of paMELA, Section III presents the simulation results from a complete cross-domain model of the system and its performance characterization. Finally, in Section IV conclusions will be drawn.

2 PHOTOACOUSTIC MELANOMA DETECTOR DESIGN

Photoacoustic imaging can be obtained by several techniques that can be summarized in two main categories: Photoacoustic Microscopy (PAM) exploits a single channel acoustic sensor and a focused laser beam to perform a raster scan above the sample and obtain a pixel-by-pixel image. Although the instrumentation is simple, the mechanical scanning over thousands of pixels is time consuming (several minutes) and requires the tissue under observation to be perfectly still for long periods, to evitate misalignment in the picture. For this reason, PAM is particularly suited for pre-clinical application, but it has practical limitation as a clinical tool. paMELA exploits a different technique, called Photoacoustic Tomography (PAT), that by using a multichannel acoustic sensor and dedicated acoustic imaging algorithms can acquire a 2/3D image of the sample without any movement of the sensor, relying on acoustic beam steering in digital domain.

The laser beam spot is wide enough to illuminate all the sample and for each beam pulse an acoustic image of the whole area under observation can be taken. The acquisition time are therefore very quick and multiple images can be taken and averaged at a frame rate up to thousands/sec (limited by the laser pulse repetition rate and electronic throughput).

A block scheme of the hereby presented photoacoustic imaging setup is shown in Figure 3. It is composed by a pulsed laser, a multichannel acoustic sensor (AS), an analog front-end (AFE) and DSP stages on FPGA.

2.1 Signal Generation (Laser)

The signal is generated through the thermoacoustic effect, where a rapid deposition of energy in a certain volume generates an increase in localized temperature and a consequent increase in pressure, which propagates in space like an acoustic wave. The deposition of energy occurs when the light pulse produced by the laser encounters a tissue with a high absorption coefficient (such as melanin). The melanin inside the tissue acts as sources of an acoustic wave, and by acquiring this signal with special multichannel acoustic sensors (MAS) it is possible to locate the acoustic sources and produce a 2D image of the vascularization of the biological sample. To generate an appreciable pressure signal, the pressure deposition must be fast enough to comply with the stress confinement condition, which is 20 ns for

samples of 30 μm in size. A pulse length of 15 ns has been chosen as a tradeoff between preserving the signal linearity by respecting stress confinement and improving the acoustic signal amplitude which is proportional to the energy dose deposition as in (1), where D is the dose deposition (defined as the ratio between energy deposition and mass of the absorber volume) and Γ is the Grüneisen parameter, equal to around 100 Pa/Gy for water and tissues.

$$dP = \Gamma D \quad (1)$$

A 650 nm laser diode with 10 W peak power was used to maximize the melanin absorption. The irradiated volume can be approximated as a cylinder with 3 mm diameter and 1 mm thickness. This leads to an average dose deposition of 20 mGy and 2 Pa acoustic signal amplitude. The pressure wave then propagates in space until it reaches the acoustic sensor, undergoing spherical attenuation which is proportional to the distance between the source and the sensor (5 mm), and equal to 20 dB, thus leading to 200 mPa signal at the sensor surface. Finally, the frequency of the acoustic wave is linked to the thickness of the source measured in the AS-source direction according to equation (2).

$$f = \frac{c_s}{2 BP_{FWHM}} = \frac{c_s}{2 TH_{abs}} \quad (2)$$

Thus, to achieve 30 μm resolution paMELA has to acquire signals in the 25 MHz range.

2.2 Acoustic Signal Sensing (Multichannel Acoustic Sensor)

The acoustic signal is acquired through a piezoelectric sensor array that acts as a pressure-voltage transducer through a parameter called Sensitivity, defined in equation (3).

$$V = P \cdot S \quad (3)$$

The choice of AS depends primarily on the frequency characteristics of the acoustic signal under examination. In fact it is necessary to use an AS such that its resonance frequency corresponds with the band of the signal to be observed. The signal band in turn depends on the size of the sources, as shown in the previous section. Furthermore, in order to recreate an image of the acoustic source, it is necessary to use an array of sensors. In this way the difference in the arrival times of the acoustic wave to the different sensor channels can be used to locate the source in space in 2D and to obtain an image of the same. For this reason, a 64-channel linear array with a central

frequency of 25 MHz and 2 $\mu\text{V}/\text{Pa}$ sensitivity. Knowing the sensitivity and the electrical capacity of each channel (calculated around 50 pF), it is possible to calculate the output noise power (kT/C) and the equivalent input noise of each channel, equal to 9 μVRMS and 4.5 PaRMS respectively. Considering a 64 channel array, when acoustic imaging algorithms are applied the signals from all channels are re-phased and added, reducing random noise fluctuation while preserving the (deterministic) signal amplitude, thus lowering the total noise floor by 18 dB following equation (4), for a total of 570 mPaRMS:

$$N_{64ch} = N_{1ch}/\text{sqrt}(N_{ch}) \quad (4)$$

This value indicates the background noise of the sensor and is to be compared with the amplitude of the pressure signal to obtain the SNR. It is however possible to further lower the background noise by acquiring and averaging multiple shots of the laser beam.

2.3 Analog Signal Processing (Analog Front-end)

The output signal from the acoustic sensor is typically in the range of a fraction of μV amplitude for 200 mPa pressure at the sensor surface and 2 $\mu\text{V}/\text{Pa}$ sensitivity. Therefore it must be amplified by about 60-80 dB before being converted into the digital domain. Piezoelectric acoustic sensors are typically characterized by a very low spectral density of noise output power, therefore they require dedicated electronics that allow to obtain an acceptable noise figure (NF) while preserving the signal quality. In particular, the spectral density of noise power for the sensor used is about 2 $\text{nV}/\sqrt{\text{Hz}}$. Commercial operational amplifiers with BJT or JFET inputs allow to achieve in-band noise PSD around 1 $\text{nV}/\sqrt{\text{Hz}}$, thus achieving 1 dB NF (Vallicelli, 2020). A dedicated Low-Pass Filter is then used to reject out-of-band noise and interferers. Finally, ADC converts the signal into digital domain for signal processing.

2.4 Digital Signal Processing (Beamforming)

The DSP stages have two main goal, that are to further improve the SNR by averaging signals from multiple laser pulses and to implement acoustic imaging algorithms to obtain information about the suspect melanoma. A Delay&Sum beamforming exploits the different acoustic wave time of arrival to obtain an acoustic image of the source.

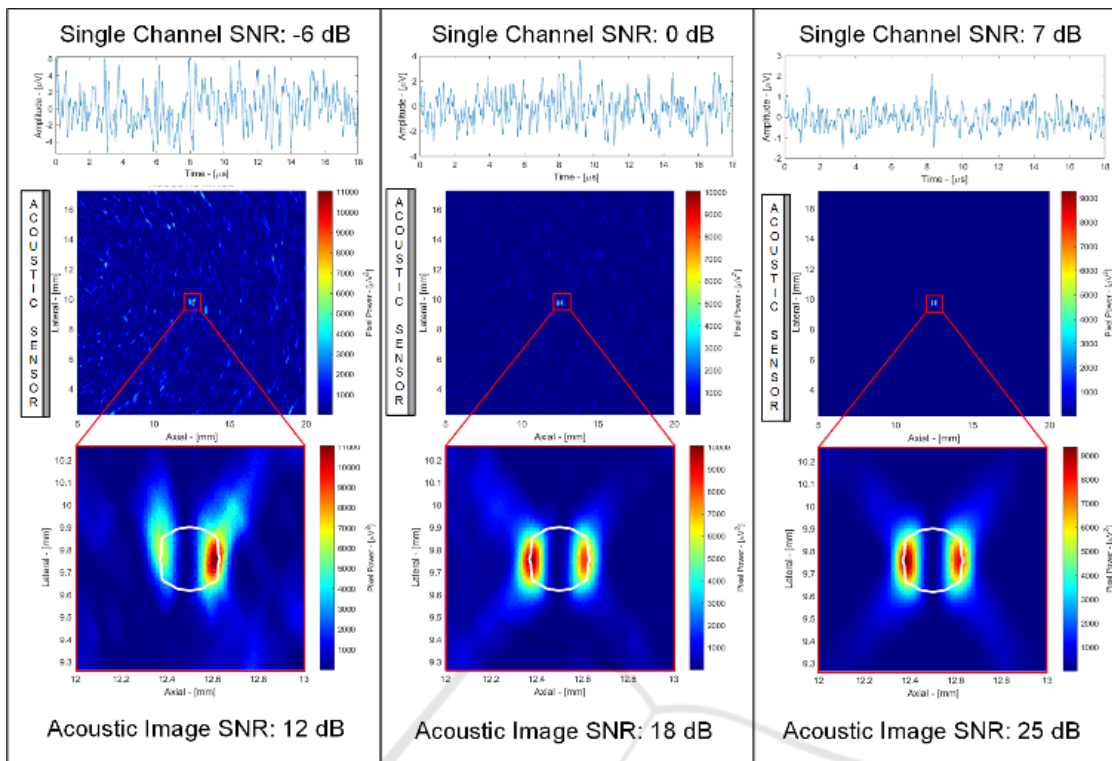


Figure 4: Single spherical source testbench.

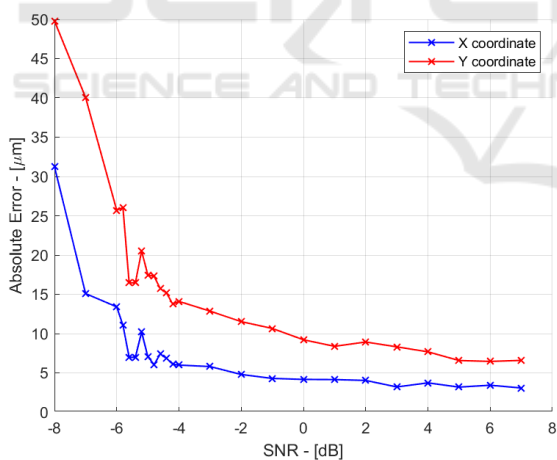


Figure 5: Localization precision performances vs. single channel SNR.

For every pixel of the acoustic image, the signals from each channel are re-phased according to the relative pixel-channel distance to highlight acoustic sources located inside the pixel and reject other sources by destructive interference. By repeating the process for each pixel (changing the re-phasing delays) an acoustic image is obtained.

3 SIMULATION RESULTS

To evaluate performance, a cross-domain model of the whole system was made using k-Wave and Matlab. The model includes the deposition of energy in space due to the laser, the generation and propagation of the acoustic wave from the source to the sensor (including attenuation and absorption effects), the noise power and frequency response of the sensor and AFE and finally the A/D conversion and DSP. This complete model allows to evaluate the performance of the system before physically creating it, in order to have a benchmark to validate the performance of the setup in the future.

3.1 Point-like Source and Performance Evaluation

To evaluate the performance of the system in terms of resolution and SNR, a single spherical source was considered placed in the centre of the observation area (Figure 4). The performance of the system was assessed in a low, medium and high SNR case to estimate the ability of the system to locate the position of the source (in two dimensions) and reconstruct its dimensions (in the axial and lateral direction) (Fig. 5).

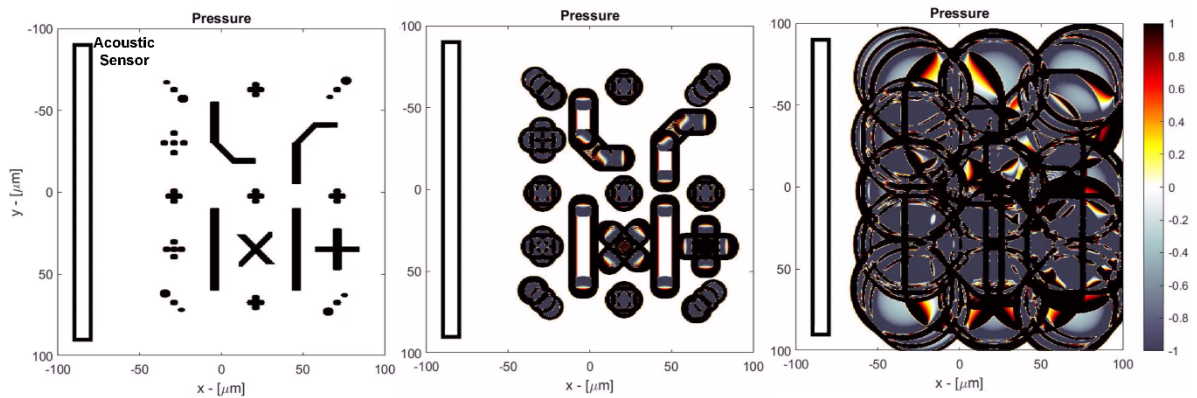


Figure 6: Time domain simulation of biological phantom.

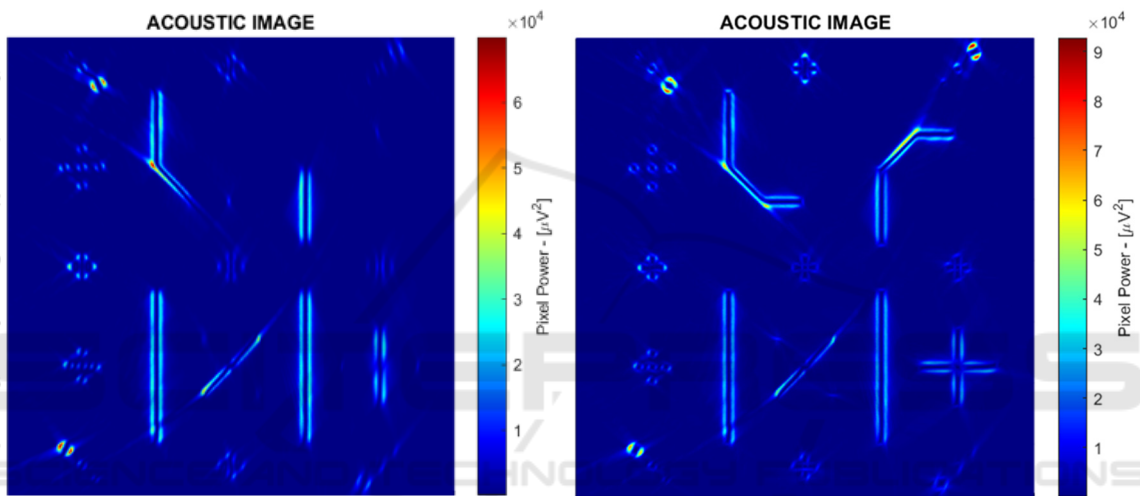


Figure 7: Final acoustic image with linear (left) and C-shaped (right) sensor.

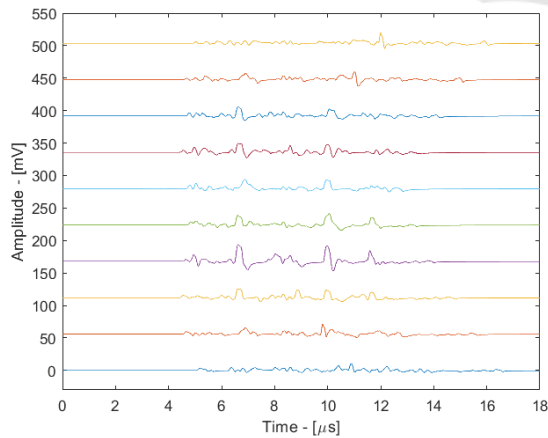


Figure 8: Time-domain output signals without noise (10 channels).

In Figure 4 the acoustic signal time track (including the noise of the sensor and electronics) acquired by the central channel of the sensor is

shown. The signal-to-noise ratio in the three cases is -6 dB, 0 dB and 7 dB respectively. By combining the signals of the 64 channels, an 18 dB increase in SNR is obtained, bringing the final value in the acoustic image to 12 dB, 18 dB and 25 dB respectively. Looking at the acoustic images, it can be seen that in all cases it is possible to clearly locate the source, distinguishing it from the background noise, although in the case of low SNR the random fluctuations due to noise are clearly visible. It is interesting to note that the size in the image of these random fluctuations have dimensions comparable to the acoustic source (and not less) due to the fact that the lowpass filter limits the high frequency noise components, which would in turn generate random fluctuations in the image with a scale smaller than that of the source.

The precision in the localization of the centre of the source was assessed by varying the SNR by repeating 100 times the position measurement in the presence of different noise realizations (always with the same SNR) and calculating the variance of the

result. Figure 5 shows how the accuracy in axial (X) and lateral localization (Y) varies with the SNR (Vallicelli, 2021). With 1kpulse/sec, 1 second acquisition allows averaging 1000 samples, leading to a single channel SNR of 0 dB (18 dB final detector SNR) and <10 μ m precision.

3.2 Biological Phantom Simulation

Finally, paMELA has been validated using a biological phantom simulation composed of several pint-like and cylindrical sources in different locations of the imaging area. The time domain simulation of such testbench is shown in Figure 6 where a linear array sensor is placed in the left. Figure 7 (left) shows the resulting acoustic image where the D&S algorithm highlights the edges of the pressure sources. It is possible to observe that the sources parallel to the sensor are clearly visible, while the sources located at an angle are fainter. This happens because linear sources irradiate acoustic energy mainly perpendicular to their direction and thus most of the acoustic wave might not be acquired by a linear sensor. To overcome this issue, Figure 7 (right) shows the results of a curved C-shaped sensor that improves the angle of observation, making all the sources clearly visible. Finally, Figure 8 shows the time-domain signals from 10 channels (one every 6) that have been used to generate the acoustic images.

4 CONCLUSIONS

This paper presents the preliminary design and complete cross-domain simulation validation of paMELA, a compact photoacoustic detector optimized for fast melanoma imaging. Through the complete characterization and design of dedicated detectors it is possible to increase the performance of these instruments to provide dermatologists with an additional tool for the early diagnosis of melanoma. paMELA manages to obtain a clear image of an area of 7 mm² in one second, obtaining 18 dB SNR and a precision of 10 μ m using a simple laser diode of 10 W of peak power.

ACKNOWLEDGEMENTS

This work has been supported by the Proton Sound Detector (ProSD) Project (founded by the Italian Institute for Nuclear Physics, INFN) and the paMELA – Photoacoustic Melanoma Detector project (co-founded by University of Milano –

Bicocca, BiUniCrowd crowdfunding campaign and Carolina Zani Melanoma Foundation).

REFERENCES

- Stewart, B. W., & Kleihues, P. (Eds.). (2003). World cancer report.
- Zhou, Y., Xing, W., Maslov, K. I., Cornelius, L. A., & Wang, L. V. (2014). Handheld photoacoustic microscopy to detect melanoma depth in vivo. *Optics letters*, 39(16), 4731-4734.
- Sinnamon, A. J., Neuwirth, M. G., Song, Y., Schultz, S. M., Liu, S., Xu, X., & Karakousis, G. C. (2019). Multispectral photoacoustic imaging for the detection of subclinical melanoma. *Journal of surgical oncology*, 119(8), 1070-1076.
- Wang, Y., Xu, D., Yang, S., & Xing, D. (2016). Toward in vivo biopsy of melanoma based on photoacoustic and ultrasound dual imaging with an integrated detector. *Biomedical optics express*, 7(2), 279-286.
- Park, B., Bang, C. H., Lee, C., Han, J. H., Choi, W., Kim, J., ... & Kim, C. (2021). 3D wide - field multispectral photoacoustic imaging of human melanomas in vivo: a pilot study. *Journal of the European Academy of Dermatology and Venereology*, 35(3), 669-676.
- Vallicelli, E. A., Turossi, D., Gelmi, L., Baù, A., Bertoni, R., Fulgione, W., ... & De Matteis, M. (2020). A 0.3 nV/ $\sqrt{\text{Hz}}$ input-referred-noise analog front-end for radiation-induced thermo-acoustic pulses. *Integration*, 74, 11-18.
- Vallicelli, E. A., & De Matteis, M. (2021). Analog Filters Design for Improving Precision in Proton Sound Detectors. *Journal of Low Power Electronics and Applications*, 11(1), 12.